

行政院國家科學委員會專題研究計畫 成果報告

以 GDQ 法做層疊壓電板殼的電腦計算

計畫類別：個別型計畫

計畫編號：NSC92-2212-E-164-007-

執行期間：92 年 08 月 01 日至 93 年 07 月 31 日

執行單位：修平技術學院資訊管理系

計畫主持人：洪志強

報告類型：精簡報告

處理方式：本計畫可公開查詢

中 華 民 國 93 年 7 月 13 日

以 GDQ 法做層疊壓電板殼的電腦計算

(Computer Approach of Laminated Piezoelectric Shells by the GDQ Method)

摘要

我們採用二維 GDQ 一般化微分級數的電腦計算數值方法，來研究具有剪應變影響之層疊壓電板殼受電壓、壓力及四邊簡支條件下之應力變化情況。我們選用一代表混合板殼，其含有 3 層直交 [90°/0°/90°] 石墨樹脂板殼及外層 PVDF 板殼的材料，來做受到正弦壓力及電壓之作用的數值分析，首先將含有一階剪應變理論(FSDT)的位移函數統御偏微分方程式，用 GDQ 方法將它寫成級數形式的方程式，再得到一些 \bar{W} 位移比， $\bar{\sigma}_x$ ， $\bar{\sigma}_\theta$ 應力比的電腦數值解。

關鍵詞：一般化微分級數、層疊壓電板殼、位移比、應力比。

Abstract

A piezoelectric laminated cylindrical shell with shear rotations effect under the electromechanical loads and four sides simply supported boundary condition was studied by using the two-dimensional generalized differential quadrature (GDQ) computational method. The typical hybrid composite shells with 3-layered cross-ply [90°/0°/90°] graphite-epoxy laminate and bounded PVDF layers are considered under the sinusoidal pressure loads and electric potentials on the shell. The governing partial differential equation with First-order Shear Deformation Theory (FSDT) in terms of mid-surface displacements and shear rotations can be expressed in series equations by the GDQ formulation. Thus we obtain the GDQ numerical solutions of displacement ratio \bar{W} , stress ratios $\bar{\sigma}_x$ and $\bar{\sigma}_\theta$.

Keywords: generalized differential quadrature (GDQ), piezoelectric laminated cylindrical shell, displacement ratio, stress ratios.

1. 前言

近年來壓電材料已經被使用及應用在如智慧結構、微機電系統、工程、超音波與醫療影像設備上。關於層疊壓電板殼的研究方面，有 Kapuria, Sengupta 和 Dumir [6-7]分別在 1998 年以 Navier-type 的作法和在 1997 年以 Exact Analytical Fourier Series 的作法得到一些位移、應力的數值解。在 1998 年 Mirfakhraei 和 Redekop 以 Differential Quadrature Method (DQM) 的數值方法做圓柱形板殼之挫曲分析[8]。在層疊壓電板殼的一般化微分級數(Generalized Differential Quadrature ,GDQ)電腦計算方法之研究方面，到目前尚未有文獻發表。

2. 研究目的

利用 GDQ 電腦計算數值方法來做層疊壓電板殼在受到表面壓力、電壓和邊界條件下的應力函數、變形函數分佈之電腦數值計算分析。

3. 文獻探討

在 2002 年，有 Liu 和 Fan 以邊界元素法(Boundary Element Method, BEM)做智慧材料、微機電系統之薄層的數值解分析[1]。Jun 和 Zhaowei 以有限元素法(Finite Element Method, FEM)做電腦硬碟系統之 PZT 壓電微驅動器的數值解研究[2]。Dubus, Haw, Granger 和 Ledez 做高功率變頻器的壓電陶瓷材料實驗[3]。在 2000 年，Benjeddou 做壓電實體、板殼、板、樑等 adaptive 材料的有限元素法研究[4]。在 1998 年，Khutoryansky, Sosa 和 Zu 以邊界元素法做 active 壓電材料的研究[5]。目前尚有一些主題仍未被發表如：曲線板殼、剪力作用機構、內流體負載結構等。在 2000 年，我們已經成功地利用二維的 GDQ 數值方法[17-19]來做複材層疊板之熱彎曲的應力分析[20]。在 1999-2001 年，我們也成功地利用應力函數法和有限差分法等方法做複材層疊板的層間應力分析[21-24]。在 2003 年，我們用 GDQ 數直方法分別對含有剪應變之層疊板做熱彎曲及熱振動的研究分析[25-26]。

4. 研究方法

Basically, the GDQ method can be stated that: the derivative of a smooth function at a discrete point in a domain can be discretized by using an approximated weighting linear sum of the function values at all the discrete points in the direction [9-16].

We use the following non-dimensionalized parameter: $X = \frac{x}{a}$, $Y = \frac{\theta}{\psi}$, $U = \frac{u^0}{a}$, $V = \frac{u^0}{h^*}$,

$W = \frac{w^0}{h^*}$. And after substituting the discretized discretized equations of governing equations, we have the discretized equations of piezoelectric shell for the stresses and the electric potential function in the grid point (i, j) as follows:

$$\begin{aligned} & \frac{(A_{11} + \bar{B}_{11})}{a} \sum_{\lambda=1}^N A_{i,\lambda}^{(2)} U_{\lambda,j} + \frac{a(A_{66} - \bar{B}_{66} + \bar{D}_{66})/R^2}{\psi^2} \sum_{m=1}^M B_{j,m}^{(2)} U_{i,m} + \frac{h^*(A_{12} + A_{66})/R}{a\psi} \sum_{\lambda=1}^N A_{i,\lambda}^{(1)} \sum_{m=1}^M B_{j,m}^{(1)} V_{\lambda,m} \\ & + \frac{h^* A_{12}/R}{a} \sum_{\lambda=1}^N A_{i,\lambda}^{(1)} W_{\lambda,j} + \frac{B_{11} + D_{11}/R}{a^2} \sum_{\lambda=1}^N A_{i,\lambda}^{(2)} \phi_{1,\lambda,j} + \frac{(\bar{B}_{66} - \bar{D}_{66})/R}{\psi^2} \sum_{m=1}^M B_{j,m}^{(2)} \phi_{1,i,m} \\ & + \frac{\bar{B}_{12} + \bar{B}_{66}}{a\psi} \sum_{\lambda=1}^N A_{i,\lambda}^{(1)} \sum_{m=1}^M B_{j,m}^{(1)} \phi_{2,\lambda,m} = -P_{x_{o,j}} - \frac{1}{a} \sum_{\lambda=1}^N A_{i,\lambda}^{(1)} N_{x_{\lambda,j}}^e \\ & \frac{a(A_{12} + A_{66})/R}{a\psi} \sum_{\lambda=1}^N A_{i,\lambda}^{(1)} \sum_{m=1}^M B_{j,m}^{(1)} U_{\lambda,m} + \frac{h^*(A_{66} + \bar{B}_{66})}{a^2} \sum_{\lambda=1}^N A_{i,\lambda}^{(2)} V_{\lambda,j} \\ & + \frac{h^*(A_{22} - \bar{B}_{22} + \bar{D}_{22})/R^2}{\psi^2} \sum_{m=1}^M B_{j,m}^{(2)} V_{i,m} + \frac{h^*(\bar{B}_{44} - \bar{D}_{44} - A_{44})}{R^2} V_{i,j} \\ & + \frac{h^*(A_{44} - \bar{B}_{44} + \bar{D}_{44} + A_{22} - \bar{B}_{22} + \bar{D}_{22})/R^2}{\psi} \sum_{m=1}^M B_{j,m}^{(1)} W_{i,m} + \frac{(\bar{B}_{12} + \bar{B}_{66})}{a\psi} \sum_{\lambda=1}^N A_{i,\lambda}^{(1)} \sum_{m=1}^M B_{j,m}^{(1)} \phi_{1,\lambda,m} \end{aligned}$$

$$\begin{aligned}
& + \frac{B_{66} + D_{66}/R}{a^2} \sum_{\lambda=1}^N A_{i,\lambda}^{(2)} \phi_{2_{\lambda,j}} + \frac{(\bar{B}_{22} - \bar{D}_{22})/R}{\psi^2} \sum_{m=1}^M B_{j,m}^{(2)} \phi_{2_{i,m}} + \frac{\bar{B}_{44} - \bar{D}_{44} - A_{44}}{-R^2} \phi_{2_{i,j}} \\
& = -P_{\theta_{i,j}} - \frac{1}{R} (Q_{\theta_{i,j}}^e + \frac{1}{\psi} \sum_{m=1}^M B_{j,m}^{(1)} N_{\theta_{i,m}}^e) \\
& \frac{a A_{12}/R}{a} \sum_{\lambda=1}^N A_{i,\lambda}^{(1)} U_{\lambda,j} + \frac{h^*(A_{44} - \bar{B}_{44} + \bar{D}_{44} + A_{22} - \bar{B}_{22} + \bar{D}_{22})/R^2}{\psi} \sum_{m=1}^M B_{j,m}^{(1)} V_{i,m} \\
& + \frac{h^*(-A_{55} - \bar{B}_{55})}{a^2} \sum_{\lambda=1}^N A_{i,\lambda}^{(2)} W_{\lambda,j} + \frac{h^*(\bar{B}_{44} - \bar{D}_{44} - A_{44})/R^2}{\psi^2} \sum_{m=1}^M B_{j,m}^{(2)} W_{i,m} \\
& + h^*(A_{22} - \bar{B}_{22} + \bar{D}_{22})/R^2 W_{i,j} + \frac{(\bar{B}_{12} - \bar{B}_{55} - A_{55})}{a} \sum_{\lambda=1}^N A_{i,\lambda}^{(1)} \phi_{1_{\lambda,j}} \\
& + \frac{(\bar{B}_{22} + \bar{B}_{44} - A_{44} - \bar{D}_{22} - \bar{D}_{44})/R}{\psi} \sum_{m=1}^M B_{j,m}^{(1)} \phi_{2_{i,m}} = P_{z_{i,j}} + \frac{1}{a} \sum_{\lambda=1}^N A_{i,\lambda}^{(1)} Q_{x_{\lambda,j}}^e + \frac{1}{R} (\frac{1}{\psi} \sum_{m=1}^M B_{j,m}^{(1)} Q_{\theta_{i,m}}^e - N_{\theta_{i,j}}^e) \\
& \frac{(B_{11} + D_{11}/R)}{a} \sum_{\lambda=1}^N A_{i,\lambda}^{(2)} U_{\lambda,j} + \frac{a(\bar{B}_{66} - \bar{D}_{66})/R}{\psi^2} \sum_{m=1}^M B_{j,m}^{(2)} U_{i,m} + \frac{h^*(\bar{B}_{12} + \bar{B}_{66})}{a\psi} \sum_{\lambda=1}^N A_{i,\lambda}^{(1)} \sum_{m=1}^M B_{j,m}^{(1)} V_{\lambda,m} \\
& + \frac{h^*(\bar{B}_{12} - \bar{B}_{55} - A_{55})}{a} \sum_{\lambda=1}^N A_{i,\lambda}^{(1)} W_{\lambda,j} + \frac{D_{11}}{a^2} \sum_{\lambda=1}^N A_{i,\lambda}^{(2)} \phi_{1_{\lambda,j}} + \frac{\bar{D}_{66}}{\psi^2} \sum_{m=1}^M B_{j,m}^{(2)} \phi_{1_{i,m}} + (-A_{55} - \bar{B}_{55}) \phi_{1_{i,j}} \\
& + \frac{(-A_{55} - \bar{B}_{55})}{a\psi} \sum_{\lambda=1}^N A_{i,\lambda}^{(1)} \sum_{m=1}^M B_{j,m}^{(1)} \phi_{2_{\lambda,m}} = -m_{x_{i,j}} + Q_{x_{i,j}}^e - \frac{1}{a} \sum_{\lambda=1}^N A_{i,\lambda}^{(1)} M_{x_{\lambda,j}}^e \\
& \frac{a(\bar{B}_{12} + \bar{B}_{66})}{a\psi} \sum_{\lambda=1}^N A_{i,\lambda}^{(1)} \sum_{m=1}^M B_{j,m}^{(1)} U_{\lambda,m} + \frac{h^*(B_{66} + D_{66}/R)}{a^2} \sum_{\lambda=1}^N A_{i,\lambda}^{(2)} V_{\lambda,j} + \frac{h^*(\bar{B}_{22} - \bar{D}_{22})/R}{\psi^2} \sum_{m=1}^M B_{j,m}^{(2)} V_{i,m} \\
& + \frac{h^*(\bar{B}_{44} - \bar{D}_{44} - A_{44})}{-R} V_{i,j} + \frac{(\bar{B}_{22} + \bar{B}_{44} - A_{44} - \bar{D}_{22} - \bar{D}_{44})/R}{\psi} \sum_{m=1}^M B_{j,m}^{(1)} W_{i,m} \\
& + \frac{(-A_{55} - \bar{B}_{55})}{a\psi} \sum_{\lambda=1}^N A_{i,\lambda}^{(1)} \sum_{m=1}^M B_{j,m}^{(1)} \phi_{1_{\lambda,m}} + \frac{D_{66}}{a^2} \sum_{\lambda=1}^N A_{i,\lambda}^{(2)} \phi_{2_{\lambda,j}} + \frac{\bar{D}_{22}}{\psi^2} \sum_{m=1}^M B_{j,m}^{(2)} \phi_{2_{i,m}} + (\bar{B}_{44} - \bar{D}_{44} - A_{44}) \phi_{2_{i,j}} \\
& = -m_{\theta_{i,j}} + Q_{\theta_{i,j}}^e - \frac{1}{\psi R} \sum_{m=1}^M B_{j,m}^{(1)} M_{\theta_{i,m}}^e
\end{aligned}$$

And the terms of the contribution to force and moment resultants due to applied electric field $E = [E_x, E_\theta, E_z]^T$ are given for the N_k layers. $E_x = -\phi_{,x}$, $E_\theta = -\phi_{,\theta}/(R+Z)$, $E_z = -\phi_{,z}$

where ϕ_1 and ϕ_2 are the electric potentials at the inner and outer surfaces of the shell. The potentials ϕ are assumed to vary linearly across the layers of shell, $\phi = \phi_1 + z\phi_2$.

5. 結果與討論

一般化微分級數(GDQ)法可提供我們在研究混合層疊壓電板殼受到表面壓力、電壓和簡支邊界條件下的電腦計算解。我們得到了一些在混合層疊壓電板殼之中央位置的 \bar{W} 位移比, $\bar{\sigma}_x$, $\bar{\sigma}_\theta$ 應力比分別對厚度-中表面半徑比和長度-中表面半徑比的變化情形，並討論如下：

In order to obtain some numerical GDQ results in personal computer, we consider the hybrid composite shell made of cross-ply graphite-epoxy laminate and PVDF (polyvinylidene fluoride) layer bonded to its surface. The typical hybrid composite shell is listed as follows:

Type1: 3-layered cross-ply graphite-epoxy laminate [$90^\circ/0^\circ/90^\circ$] and an outer PVDF layer.

Type2: 3-layered cross-ply graphite-epoxy laminate [$90^\circ/0^\circ/90^\circ$] and PVDF layers bonded to its inner and outer surfaces.

The material properties of graphite-epoxy are given as follows [6]:

$$E_L = 172.5 \text{ GPa}, E_T = 6.9 \text{ GPa}, G_{LT} = 3.45 \text{ GPa}, G_{TT} = 1.38 \text{ GPa}, \gamma_{LT} = \gamma_{TT} = 0.25, d_i = 0.$$

And the material properties of PVDF are given as follows[6]:

$$E_i = 2.0 \text{ GPa}, \gamma_{ij} = \frac{1}{3}, d_1 = 3 \times 10^{-12} \text{ CN}^{-1}, d_2 = 23 \times 10^{-12} \text{ CN}^{-1}, d_3 = -30 \times 10^{-12} \text{ CN}^{-1}, d_4 = 0, d_5 = 0.$$

We consider the typical hybrid shell (see Figure1) including shear deformation under four sides simply supported for the following electromechanical loads cases with $P_x = P_\theta = m_x = 0$:

$$\text{case1: } P_z = -P_0(1 + \frac{h^*}{2R}) \sin(\frac{\pi x}{a}) \cos \theta, \phi_1 = \phi_2 = 0$$

$$\text{case2: } P_z = 0, \phi_1 = 0, \phi_2 = \phi_0 \sin(\frac{\pi x}{a}) \cos \theta$$

And we use the following coordinate of grid points in the GDQ computation:

$$x_i = 0.5 \left[1 - \cos\left(\frac{i-1}{N-1}\pi\right) \right] a, i = 1, 2, K, N, \theta_i = 0.5 \left[1 - \cos\left(\frac{j-1}{M-1}\pi\right) \right] \psi, j = 1, 2, K, M.$$

We firstly make the convergence study of deflection W at center position for type1 hybrid shell under case1 load with $P_0 = 1.0 \text{ MPa}$, all plies of hybrid shell have equal thickness, span angle of the panel $\psi = 120^\circ$, length-to-midsurface radius ratio $\frac{a}{R} = 1, 2, 3, 4$ and thickness-to-midsurface radius

ratio $\frac{h^*}{R} = 0.01, 0.05, 0.1, 0.17, 0.25$. The non-dimensional deflection W at center position type1 hybrid shell in GDQ method for the grid point $N \times M = 5 \times 5, 9 \times 9, 13 \times 13, 15 \times 15, 19 \times 19, 23 \times 23, 27 \times 27$ and 31×31 is presented in the Table1. We find that the 31×31 grid point have a good convergence result and can be used further for the hybrid shell including shear deflection analyses under the electromechanical loads and four sides simply supported.

The displacement ratio $\bar{W} = \frac{W}{W|_{\frac{h^*}{R}=0.01}}$, and stress ratios $\bar{\sigma}_x = \frac{\sigma_x}{\sigma_x|_{\frac{h^*}{R}=0.01}}, \bar{\sigma}_\theta = \frac{\sigma_\theta}{\sigma_\theta|_{\frac{h^*}{R}=0.01}}$ are

defined and used for the following Figures, all the non-dimensional deflection and stress parameters are compared to the corresponding values at $\frac{h^*}{R} = 0.01$.

Figure 2 shows that the variation of the non-dimensional parameters $\bar{W}, \bar{\sigma}_x$ and $\bar{\sigma}_\theta$ with the $\frac{h^*}{R}$ at center position of hybrid shell. Type1 under load case1: $P_z = -P_0(1 + \frac{h^*}{2R}) \sin(\frac{\pi x}{a}) \cos \theta$, $P_0 = 1.0 \text{ MPa}, \phi_1 = \phi_2 = 0$ and $\frac{a}{R} = 4, W|_{\frac{h^*}{R}=0.01} = 0.02525, \sigma_x|_{\frac{h^*}{R}=0.01} = 0.04455, \sigma_\theta|_{\frac{h^*}{R}=0.01} = 1.24117$.

We find that $\bar{W}, \bar{\sigma}_x$ and $\bar{\sigma}_\theta$ are all decreasing with $\frac{h^*}{R}$ increasing, especially in the region $\frac{h^*}{R} < 0.05$.

Figure 3 shows that the variation of the non-dimensional parameters $\bar{W}, \bar{\sigma}_x$ and $\bar{\sigma}_\theta$ with the $\frac{a}{R}$ at center position of hybrid shell. Type1 under load case1: $P_z = -P_0(1 + \frac{h^*}{2R}) \sin(\frac{\pi x}{a}) \cos \theta$,

$P_0 = 1.0 \text{ MPa}, \phi_1 = \phi_2 = 0$ and $\frac{h^*}{R} = 0.01$, for the computational value at center position of hybrid shell Type1, $W|_{\frac{h^*}{R}=0.01} = 0.02525, \sigma_x|_{\frac{h^*}{R}=0.01} = 0.04455, \sigma_\theta|_{\frac{h^*}{R}=0.01} = 1.24117$. We find that \bar{W} is almost

constant with $\frac{a}{R}$, $\bar{\sigma}_x$ and $\bar{\sigma}_\theta$ are all decreasing with $\frac{a}{R}$ increasing.

Figure 4 shows that the variation of the non-dimensional parameters \bar{W} , $\bar{\sigma}_x$ and $\bar{\sigma}_\theta$ with the $\frac{h^*}{R}$ at center position of hybrid shell. Type1 under load case2: $p_z = 0$, $\phi_1 = 0$, $\phi_2 = \phi_0 \sin(\frac{\pi x}{a}) \cos \theta$ and $\frac{a}{R} = 4$ for the computational value at center position of hybrid shell Type2, $W|_{\frac{h^*}{R}=0.01} = 0.390167$, $\sigma_x|_{\frac{h^*}{R}=0.01} = 0.727941$, $\sigma_\theta|_{\frac{h^*}{R}=0.01} = 19.1634$. We find that \bar{W} is decreasing with $\frac{h^*}{R}$ increasing, but $\bar{\sigma}_x$ and $\bar{\sigma}_\theta$ are increasing with $\frac{h^*}{R}$ increasing.

Figure 5 shows that the variation of the non-dimensional parameters \bar{W} , $\bar{\sigma}_x$ and $\bar{\sigma}_\theta$ with the $\frac{a}{R}$ at center position of hybrid shell. Type1 under load case2: $p_z = 0$, $\phi_1 = 0$, $\phi_2 = \phi_0 \sin(\frac{\pi x}{a}) \cos \theta$ and $\frac{h^*}{R} = 0.01$, for the computational value at center position of hybrid shell Type2, $W|_{\frac{h^*}{R}=0.01} = 0.390167$, $\sigma_x|_{\frac{h^*}{R}=0.01} = 0.727941$, $\sigma_\theta|_{\frac{h^*}{R}=0.01} = 19.1634$. We find that \bar{W} is almost constant with $\frac{a}{R}$, $\bar{\sigma}_x$ and $\bar{\sigma}_\theta$ are all decreasing with $\frac{a}{R}$ increasing.

Figure 6 shows that the variation of the non-dimensional parameters \bar{W} , $\bar{\sigma}_x$ and $\bar{\sigma}_\theta$ with the $\frac{h^*}{R}$ at center position of hybrid shell. Type2 under loads case1: $p_z = -p_0(1 + \frac{h}{2R}) \sin(\frac{\pi x}{a}) \cos \theta$, $p_0 = 1.0 Mp_a$, $\phi_1 = \phi_2 = 0$ and $\frac{h^*}{R} = 0.01$ for the computational value at center position of hybrid shell Type2, $W|_{\frac{h^*}{R}=0.01} = 0.03073$, $\sigma_x|_{\frac{h^*}{R}=0.01} = 0.4714$, $\sigma_\theta|_{\frac{h^*}{R}=0.01} = 1.12159$. We find that \bar{W} is almost constant with $\frac{h^*}{R}$, $\bar{\sigma}_x$ and $\bar{\sigma}_\theta$ are all decreasing with $\frac{h^*}{R}$ increasing.

Figure 7 shows that the variation of the non-dimensional parameters \bar{W} , $\bar{\sigma}_x$ and $\bar{\sigma}_\theta$ with the $\frac{a}{R}$ at center position of hybrid shell. Type2 under loads case1: $p_z = -p_0(1 + \frac{h^*}{2R}) \sin(\frac{\pi x}{a}) \cos \theta$, $p_0 = 1.0 Mp_a$, $\phi_1 = \phi_2 = 0$ and $\frac{h^*}{R} = 0.01$, for the computational value at center position of hybrid shell Type2, $W|_{\frac{h^*}{R}=0.01} = 0.390167$, $\sigma_x|_{\frac{h^*}{R}=0.01} = 0.727941$, $\sigma_\theta|_{\frac{h^*}{R}=0.01} = 19.1634$. We find that \bar{W} is almost constant with $\frac{a}{R}$, $\bar{\sigma}_x$ and $\bar{\sigma}_\theta$ are all decreasing with $\frac{a}{R}$ increasing.

Figure 8 shows that the variation of the non-dimensional parameters \bar{W} , $\bar{\sigma}_x$ and $\bar{\sigma}_\theta$ with the $\frac{h^*}{R}$ at center position of hybrid shell. Type2 under loads case2: $p_z = 0$, $\phi_1 = 0$, $\phi_2 = \phi_0 \sin(\frac{\pi x}{a}) \cos \theta$ and

$\frac{a}{R} = 4$ for the computational value at center position of hybrid shell Type2, $W\Big|_{\frac{h^*}{R}=0.01} = 0.03073$, $\sigma_x\Big|_{\frac{h^*}{R}=0.01} = 0.4714$, $\sigma_\theta\Big|_{\frac{h^*}{R}=0.01} = 1.12159$. We find that \bar{W} is decreasing with $\frac{h^*}{R}$ increasing, $\bar{\sigma}_x$ and $\bar{\sigma}_\theta$ are all almost constant with $\frac{h^*}{R}$.

Figure 9 shows that the variation of the non-dimensional parameters \bar{W} , $\bar{\sigma}_x$ and $\bar{\sigma}_\theta$ with the $\frac{a}{R}$ at center position of hybrid shell. Type2 under loads case2: $p_z = 0$, $\phi_1 = 0$, $\phi_2 = \phi_0 \sin(\frac{\pi x}{a}) \cos \theta$ and $\frac{h^*}{R} = 0.01$ for the computational value at center position of hybrid shell Type2, $W\Big|_{\frac{h^*}{R}=0.01} = 0.75958$, $\sigma_x\Big|_{\frac{h^*}{R}=0.01} = 1.25817$, $\sigma_\theta\Big|_{\frac{h^*}{R}=0.01} = 27.7654$. We find that \bar{W} is almost constant with $\frac{a}{R}$, $\bar{\sigma}_x$ and $\bar{\sigma}_\theta$ are all decreasing with $\frac{a}{R}$ increasing.

Conclusions

The two-dimensional generalized differential quadrature (GDQ) method give us a computational solution of the laminated PVDF hybrid shell under the electromechanical loads and four sides simply supported. We obtain the variations of the non-dimensional parameters of displacement ratio \bar{W} , stress ratios $\bar{\sigma}_x$ and $\bar{\sigma}_\theta$ with respect to thickness-to-midsurface radius ratio $\frac{h^*}{R}$ and length-to-midsurface radius ratio $\frac{a}{R}$ at center position of hybrid shell.

6. 參考文獻

- [1] Liu Y. and Fan H. Analysis of thin piezoelectric solids by the boundary element method. Comput. Methods Appl. Mech. Engrg 2002; 191: 2297-2315.
- [2] Jun S. and Zhaowei Z. Finite element analysis of a IBM suspension integrated with a PZT microactuator. Sensors and Actuators 2002; A 100: 257-263.
- [3] Dubus B., Haw G., Granger C. and Ledez O. Characterization of multilayered piezoelectric ceramics for high power transducers. Ultrasonics 2002; 40: 903-906.
- [4] Benjeddou A. Advances in piezoelectric finite element modeling of adaptive structural elements: a survey. Computers and Structures 2000; 76: 347-363.
- [5] Khutoryansky N., Sosa H. and Zu W. Approximate Green's functions and a boundary element method for electro-elastic analyses of active materials. Computers and Structures 1998; 66: 289-299.
- [6] Kapuria S., Sengupta S. and Dumir P. C. Assessment of Shell Theories for Hybrid Piezoelectric Cylindrical Shell under Electromechanical Load. Int. J. Mech. Sci. 1998; Vol. 40, No. 5: 461-477.
- [7] Kapuria S., Sengupta S. and Dumir P. C. Three-dimensional Solution for Simply-supported Piezoelectric Cylindrical Shell for Axisymmetric Load. Computer Methods in Applied Mechanics and Engineering 1997; 140: 139-155.
- [8] Mirfakhraei P. and Redekop D. Buckling of Circular Cylindrical Shells by the Differential Quadrature Method. International Journal of Pressure Vessels and Piping 1998; 75: 347-353.
- [9] Bellman R.E. and Casti J. Differential Quadrature and Long-Term integration. Journal of

Mathematical Analysis and Applications 1971; Vol. 34: 235-238.

- [10] Bellman R.E. Methods of Nonlinear Analysis, 2, Academic Press, New York, 1973, chap. 16.
- [11] Bellman R.E and Kashef B.G. Solution of the Partial Differential Equation of the Hodgkins-Huxley Model Using Differential Quadrature. Mathematical Biosciences 1974; 19: 1-8.
- [12] Bellman R.E., Kashef B.G. and Casti J. Differential Quadrature: A Technique for the Rapid Solution of Non-Linear Partial Differential Equations. Journal of Computational Physics 1972; Vol. 10: 40-52.
- [13] Bellman R.E and Roth R.S. System Identification with Partial Information. Journal of Mathematical Analysis and Applications, 1979; Vol. 68: 321-333.
- [14] Bellman R.E and Roth R.S. A Scanning Technique for Systems Identification. Journal of Mathematical Analysis and Applications 1979; Vol. 71: 403-411.
- [15] Bert C. W., Jang S. K. and Striz A. G. Nonlinear Bending Analysis of Orthotropic Rectangular Plates by the Method of Differential Quadrature. Computational Mechanics 1989; 5: 217-226.
- [16] Bert C.W. and Malik M. Differential Quadrature method in Computational Mechanics: A Review. Appl Mech January 1996; Rev vol 49, no 1: 1-27.
- [17] Shu C. and Du H. Implementation of Clamped and Simply Supported Boundary Conditions in the GDQ Free Vibration Analyses of Beams and Plates. Int. J. Solids Structures 1997; Vol. 34, No. 7: 819-835.
- [18] Hua Li and Lam K.Y. Frequency Characteristic of a Thin Rotating Cylindrical Shell Using the Generalized Differential Quadrature Method. Int. J. Mech. Sci. 1998; Vol. 40, No. 5: 443-459.
- [19] Liew K. M. and Teo T. M. Modeling via Differential Quadrature Method: Three-dimensional Solutions for Rectangular plates. Computer Methods in Applied Mechanics and Engineering 1998; 159: 369-381.
- [20] Jane K. C. and Hong C. C. Thermal Bending Analysis of Laminated Orthotropic Plates by the Generalized Differential Quadrature method. Mechanics Research Communications 2000; Vol. 27, No. 2: 157-164.
- [21] Jane, K. C. Hwang, M. F. and Hong, C. C. (2001). Effect of Unsteady Aerodynamic Pressure Load on the Interlaminar Stresses of Laminated Composite Strips. International Journal of Mechanical Sciences 43, pp.1793-1812
- [22] Jane, K. C. and Hong, C. C. (2000). Interlaminar Stresses of Rectangular Laminated Plate with Simply Supported Edges Subject to Free Vibration. International Journal of Mechanical Sciences 42, pp. 2031-2039
- [23] Jane, K. C. and Hong, C. C. (2000). Buckling and Vibration of Rectangular Laminates with Cut Off Regions. Mechanics Research Communications Vol. 27, No. 1, pp. 101-108.
- [24] Jane, K. C. and Hong, C. C. (1999). Steady-State Aeroelasticity of Fluid Flow Over A Laminated Composite Plate. Mechanics Research Communications Vol. 26, No. 2, pp. 177-183.
- [25] C.C. Hong, K.C. Jane (2003), Shear Deformation in Thermal Bending Analysis of Laminated Plates by the GDQ Method, Mechanics Research Communications 30 , 2003, pp. 175-185 屬於 SCI.
- [26] C.C. Hong, K.C. Jane (2003), Shear Deformation in Thermal Vibration Analysis of Laminated Plates by the GDQ Method, International Journal of Mechanical Sciences 45, 2003, pp. 21-36 屬於 SCI.

Table1. Convergence of center deflection W for Type1 Hybrid shell:[90°/0°/90°] and an Outer PVDF case1 load: $P_z = -P_0(1 + \frac{h^*}{2R})\sin(\frac{\pi x}{a})\cos\theta$, $P_0 = 1.0MPa$, $\phi_1 = \phi_2 = 0$

a / R	GDQ Method N×M Grid points	Center deflection W				
		$\frac{h^*}{R} = 0.01$	$\frac{h^*}{R} = 0.05$	$\frac{h^*}{R} = 0.1$	$\frac{h^*}{R} = 0.17$	$\frac{h^*}{R} = 0.25$
1	5×5	0.03573	0.00146	0.000381	0.000139	0.0000692
	9×9	0.03468	0.00142	0.000369	0.000135	0.0000673
	13×13	0.03213	0.00132	0.000343	0.000126	0.0000630
	15×15	0.02555	0.00106	0.000278	0.000103	0.0000523
	19×19	0.02693	0.00111	0.000292	0.000108	0.0000544
	23×23	0.02737	0.00113	0.000297	0.000110	0.0000551
	27×27	0.02763	0.00114	0.000298	0.000110	0.0000553
	31×31	0.02753	0.00114	0.000299	0.000110	0.0000553
2	5×5	0.03248	0.00132	0.000339	0.000121	0.0000581
	9×9	0.03161	0.00128	0.000325	0.000117	0.0000564
	13×13	0.02953	0.00120	0.000308	0.000110	0.0000528
	15×15	0.02356	0.00096	0.000264	0.000088	0.0000423
	19×19	0.02495	0.00102	0.000261	0.000093	0.0000448
	23×23	0.02549	0.00104	0.000267	0.000095	0.0000457
	27×27	0.02568	0.00105	0.000269	0.000096	0.0000460
	31×31	0.02581	0.00105	0.000269	0.000096	0.0000461
3	5×5	0.03187	0.00130	0.000332	0.000118	0.0000564
	9×9	0.03104	0.00126	0.000323	0.000115	0.0000547
	13×13	0.02904	0.00118	0.000301	0.000107	0.0000508
	15×15	0.02314	0.00094	0.000241	0.000085	0.0000408
	19×19	0.02459	0.00100	0.000256	0.000091	0.0000434
	23×23	0.02511	0.00102	0.000262	0.000093	0.0000443
	27×27	0.02529	0.00103	0.000264	0.000093	0.0000447
	31×31	0.02539	0.00103	0.000264	0.000094	0.0000448
4	5×5	0.03166	0.00129	0.000330	0.000117	0.0000558
	9×9	0.03085	0.00125	0.000320	0.000114	0.0000543
	13×13	0.02887	0.00117	0.000298	0.000106	0.0000509
	15×15	0.02302	0.00094	0.000239	0.000085	0.0000402
	19×19	0.02446	0.00099	0.000254	0.000090	0.0000430
	23×23	0.02499	0.00102	0.000260	0.000092	0.0000436
	27×27	0.02519	0.00102	0.000262	0.000093	0.0000442
	31×31	0.02525	0.00102	0.000262	0.000093	0.0000444

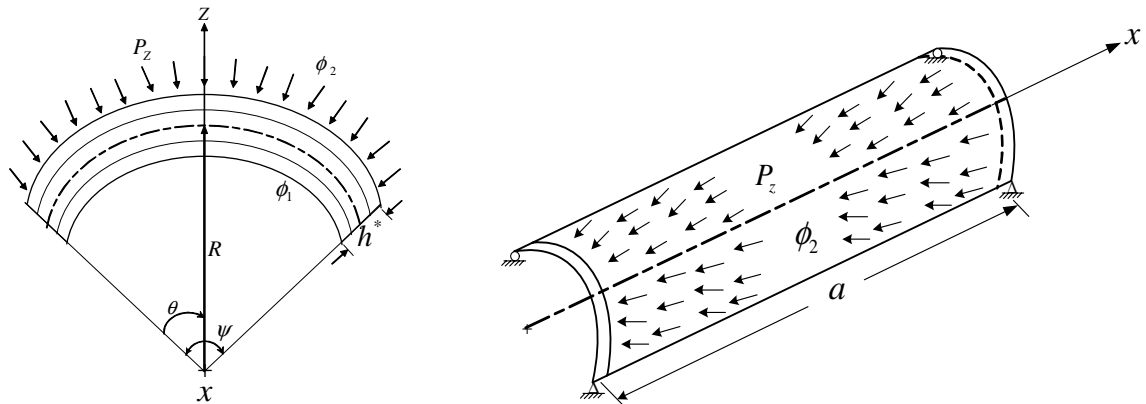


Figure 1 Typical geometry of piezoelectric cylindrical shell under pressure and electric loads.

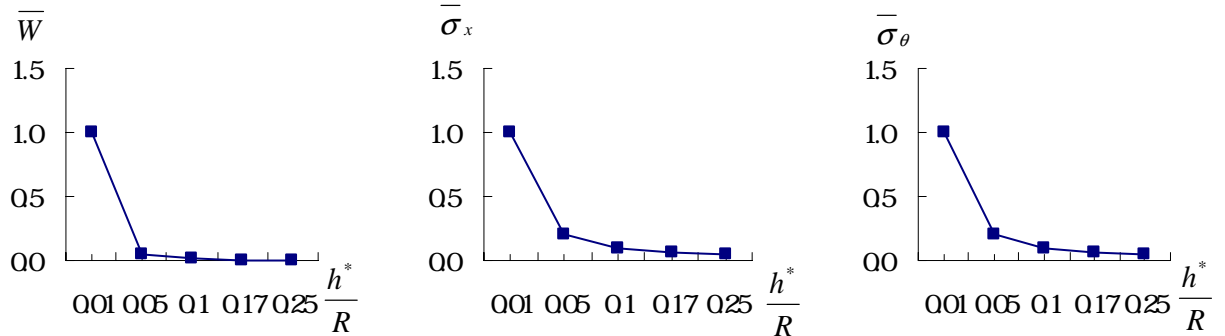


Figure 2 $\frac{h^*}{R}$ v.s $\bar{W}, \bar{\sigma}_x, \bar{\sigma}_\theta$ at center position of hybrid shell Type1 under loads case1 and $\frac{a}{R} = 4$

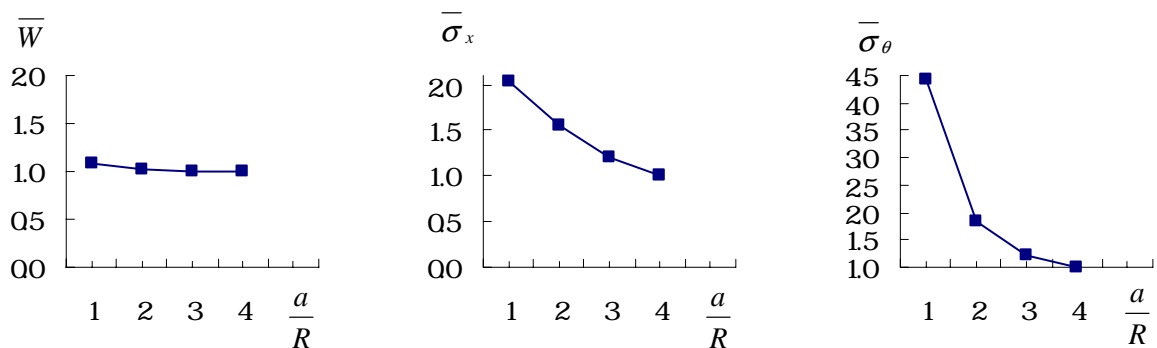


Figure 3 $\frac{a}{R}$ v.s $\bar{W}, \bar{\sigma}_x, \bar{\sigma}_\theta$ at center position of hybrid shell Type1 under loads case1 $\frac{h^*}{R} = 0.01$

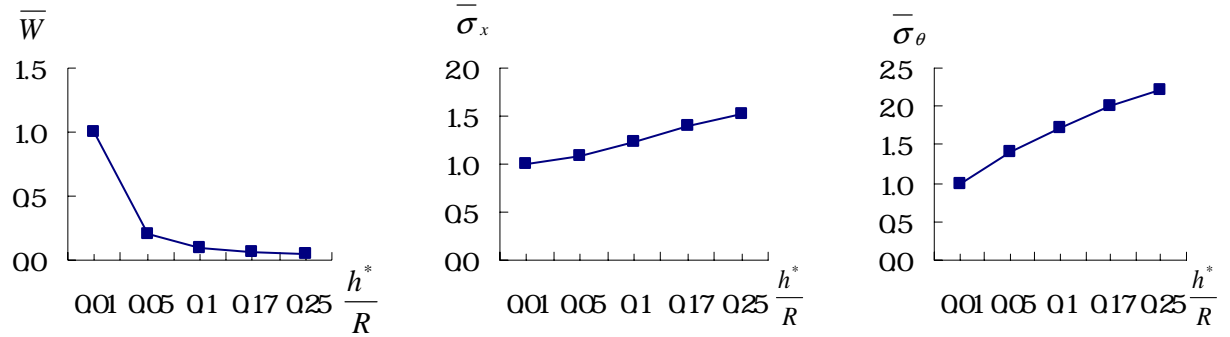


Figure 4 $\frac{h^*}{R}$ v.s $\bar{W}, \bar{\sigma}_x, \bar{\sigma}_\theta$ at center position of hybrid shell Type1 under loads case2 and $\frac{a}{R} = 4$

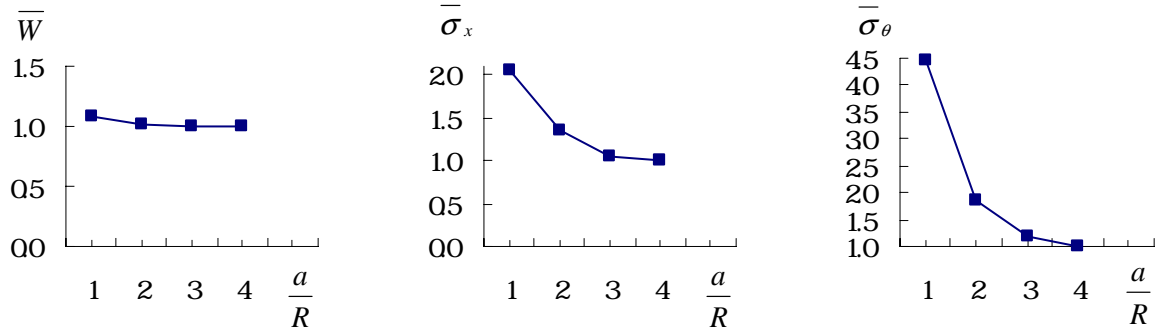


Figure 5 $\frac{a}{R}$ v.s $\bar{W}, \bar{\sigma}_x, \bar{\sigma}_\theta$ at center position of hybrid shell Type1 under loads case2 and $\frac{h^*}{R} = 0.01$

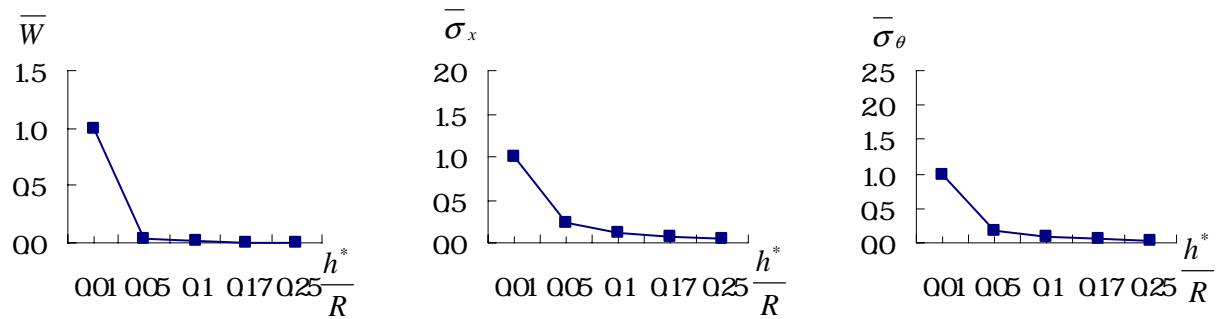


Figure 6 $\frac{h^*}{R}$ v.s $\bar{W}, \bar{\sigma}_x, \bar{\sigma}_\theta$ at center of $x - \theta$ plane and $\frac{Z}{h^*} = -0.1$ of hybrid shell Type2 under loads case1 and $\frac{h^*}{R} = 0.01$

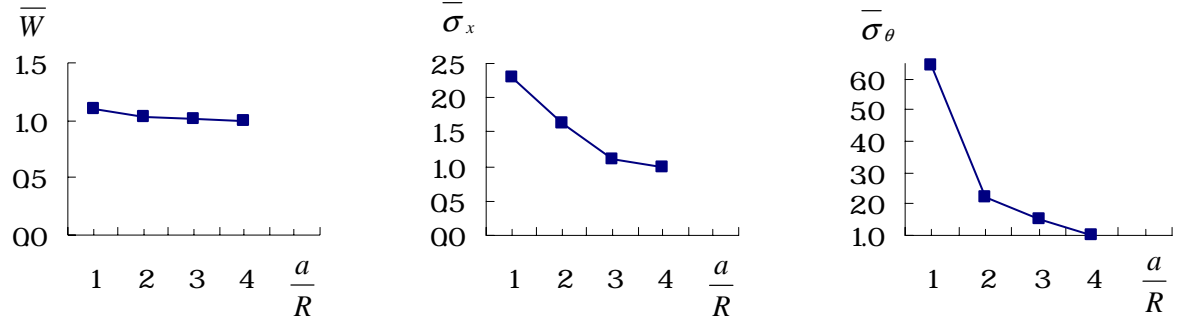


Figure 7 $\frac{a}{R}$ v.s $\bar{W}, \bar{\sigma}_x, \bar{\sigma}_\theta$ at center of $x-\theta$ plane and $\frac{Z}{h^*} = -0.1$ of hybrid shell Type2 under loads case1 and $\frac{h^*}{R} = 0.01$

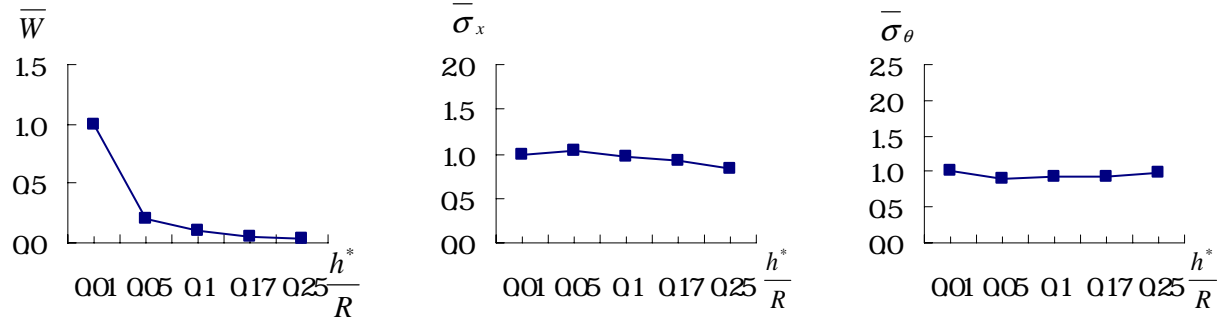


Figure 8 $\frac{h^*}{R}$ on $\bar{W}, \bar{\sigma}_x, \bar{\sigma}_\theta$ at center of $x-\theta$ plane and $\frac{Z}{h^*} = -0.1$ of hybrid shell Type2 under loads case2 and $\frac{a}{R} = 4$

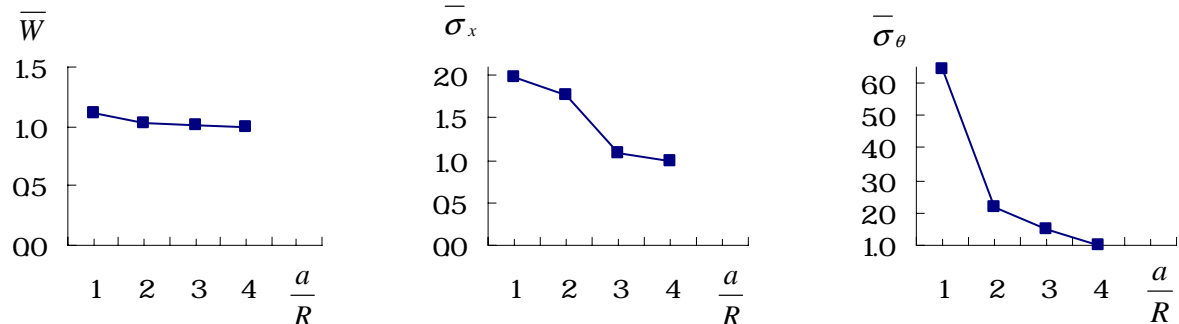


Figure 9 $\frac{a}{R}$ v.s $\bar{W}, \bar{\sigma}_x, \bar{\sigma}_\theta$ at center of $x-\theta$ plane and $\frac{Z}{h^*} = -0.1$ of hybrid shell Type2 under loads case2 and $\frac{h^*}{R} = 0.01$